Single-Molecule Nanopositioning: Structural Transitions of a Helicase-DNA Complex during ATP Hydrolysis

Hamza Balci,[†] Sinan Arslan,[†] Sua Myong,[‡§] Timothy M. Lohman,[¶] and Taekjip Ha[†‡‖*]
[†]Physics Department, [‡]Institute for Genomic Biology and [§]Department of Bioengineering, University of Illinois, Urbana, Illinois; [¶]Department of Biochemistry and Molecular Biophysics, Washington University School of Medicine, St. Louis, Missouri; and [‖]Howard Hughes Medical Institute, Chevy Chase, Maryland

ABSTRACT The conformational states of *Escherichia coli* Rep helicase undergoing ATP hydrolysis while bound to a partial-duplex DNA (pdDNA) were studied using single-molecule FRET. Crystallographic studies showed that Rep bound to single-stranded DNA can exist in open and closed conformations that differ in the orientation of the 2B subdomain. FRET measurements between eight Rep mutants donor-labeled at different residues and pdDNA acceptor-labeled at the junction were conducted at each of the four nucleotide states. The positions of donor-labeled residues, based on crystal structure, and FRET measurements between these donor molecules and the acceptor fluorophore at the DNA junction were used to predict the most likely position for the DNA junction using a triangulation algorithm. These predicted junction positions are compared with the crystal structure to determine whether the open or closed conformation is more consistent with the FRET data. Our data revealed that there are two distinct Rep-pdDNA conformations in the ATPγS and ADP states, an unexpected finding. The primary conformation is similar to that observed in nucleotide-free and ADP.Pi states, and the secondary conformation is a novel conformation where the duplex DNA and 2B subdomain moved as a unit by 13 Å relative to the rest of the protein. The primary conformation found in all nucleotide states is consistent with the closed conformation of the crystal structure however; the secondary conformation is a new conformation that has not been observed before. We discuss the possible implications of this newly observed conformation.

INTRODUCTION

Helicases use the binding, hydrolysis, and release of nucleoside triphosphates (NTPs) to unwind double-stranded DNA (dsDNA) or RNA into its complementary single strands (1–3). In addition, processive helicases translocate directionally along single-stranded DNA (ssDNA) and are thus motor proteins (4). These enzymes are involved in nearly all aspects of DNA metabolism, including replication, repair, and recombination of DNA, remodeling of chromatin, removal of proteins from DNA and RNA, and movement of Holliday junctions (1,5–9). As such, defects in helicases cause a variety of human diseases, including cancer predisposition, premature aging, and mental retardation (10).

Escherichia coli Rep is an SF1 superfamily helicase/translocase that shares extensive structural and sequence similarity with *E. coli* UvrD and *Bacillus stearothermophilus* PcrA (11–13). The monomeric forms of all three of these enzymes can translocate processively with 3′-to-5′ biased directionality along ssDNA (14–19). However, Rep, UvrD, and PcrA monomers by themselves are unable to unwind duplex DNA processively in vitro; processive unwinding activity in vitro requires the action of more than a monomer (14,18,20,21). Rep, UvrD, and PcrA monomers consist of two domains (1 and 2), each of which is composed of two subdomains, referred to as 1A and 1B and 2A and 2B. The 1A and 2A subdomains are the motor domains, also called RecA-like domains, as their folding is similar to that of the recombination protein RecA that catalyzes strand exchange between homologous DNA. The interface between 1A and 2A subdomains forms the ATP-binding domain, whereas ssDNA bridges the interface (11). Crystal structures of Rep-ssDNA complexes (12) show two distinct conformations that differ by a 130° rotation of the 2B subdomain around the hinge region that connects the 2B subdomain to the 2A subdomain (see Fig. 1, *a* and *b*). These two conformations are referred to as the open and closed conformations based on whether the large cleft formed at the interface of the four subdomains is open or closed by the 2B rotation. The position and orientation of the other three subdomains (1A, 1B, and 2A) remain essentially unchanged in the open and closed conformations. A mapping between the open and closed conformations of Rep, based on the positions of the α-carbons of the 1A, 1B, and 2A domains results in an almost perfect match, with a root-mean-squared deviation of 3.6 Å.

Similar open and closed conformations have been observed for PcrA (12,13) as well as UvrD (22,23). It is interesting that the crystal structures of PcrA and UvrD bound to a dsDNA with a short 3′ ssDNA tail both show the 2B subdomain in its closed conformation making contacts with the duplex DNA, which has led to various proposals about the significance of the 2B-subdomain-duplex-DNA interactions in DNA unwinding (13,23). However, these 2B subdomains do not contain any of the conserved helicase motifs and show significant variations in both size and sequence among

Submitted March 3, 2011, and accepted for publication July 7, 2011.

*Correspondence: tjha@illinois.edu

Hamza Balci's present address is Physics Department, Kent State University, Kent, OH 44242.

Editor: David P. Millar.

0006-3495/11/08/0976/9 $2.00

doi: 10.1016/j.bpj.2011.07.010

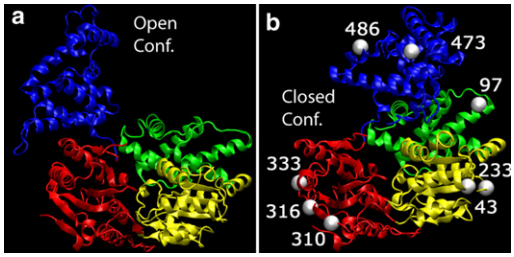

FIGURE 1 Rep structure (PDB ID 1UAA (11)) and labeling sites, showing Rep in the open (*a*) and closed (*b*) conformations, with labeled residues shown as white spheres and subdomains 1A, 2A, 1B, and 2B colored yellow, red, green, and blue, respectively.

different members of the SF1 superfamily (3). In addition, deletion of the 2B subdomain in Rep (to form RepΔ2B) does not inhibit, but rather activates, the helicase activity of the RepΔ2B monomer (14,24). Our previous solution studies of Rep bound to a dsDNA with a short 3′-ssDNA tail (referred to as partial-duplex or pdDNA), performed under nucleotide-free conditions, showed that a Rep monomer also binds to the vicinity of a ssDNA-dsDNA junction in a closed conformation (25), similar to the conformations of the PcrA and UvrD monomers observed in the crystal structures (13,23). In addition, in interactions of both PcrA and UvrD monomers with a 5′-ssDNA-duplex-DNA junction, which is not an unwinding substrate, the 2B subdomain appears to anchor the protein to the dsDNA. The anchored protein then translocates in a 3′-to-5′ direction along the ssDNA tail so that the enzyme reels in the tail, forming an ssDNA loop (26,27). Taken together, these observations were interpreted as the 2B subdomain having a regulatory, rather than a functional, role in DNA unwinding (14). In particular, it has been speculated that the interaction between the 2B subdomain and the dsDNA may function to prevent wild-type Rep monomers from unwinding or otherwise invading dsDNA (4,14). This 2B-induced unwinding inhibition and regulation may be lifted in vivo by interaction with a cellular protein partner in a context-dependent manner, but in vitro, protein-protein interaction between two or more Rep monomers is enough to suppress the proposed autoinhibitory effects of the 2B subdomain-dsDNA interaction. A detailed understanding of the 2B subdomain-duplex DNA interactions during the ATP hydrolysis cycle would facilitate an understanding of the role of these interactions. Systematic crystal structure studies, such as those reported for PcrA and UvrD complexes with DNA (13,23), are not available for the Rep helicase, making fluorescence-based assays that can probe the structure of Rep-pdDNA complexes particularly important. The studies reported here have been designed to probe the conformation of a Rep monomer in complex with pdDNA at different intermediates of ATP hydrolysis using a FRET-based assay. The crystal structure studies of Rep-ssDNA complexes (11) and our previous FRET studies on a Rep-pdDNA complex without ATP (25) serve as a basis for this study.

MATERIALS AND METHODS

DNA substrate and labeled Rep mutants

The DNA substrates were formed by annealing ssDNA of sequence 5′-Cy5-GCCTCGCTGCCGTCGCCA-Biotin-3′ with an ssDNA of sequence 5′-TG GCGACGGCAGCGAGGCTTTTTTTTTTTTTTT-3′. The ssDNA molecules were ordered from Integrated DNA Technologies (Coralville, IA). A detailed protocol of protein purification and labeling has been published elsewhere (25) and hence will not be detailed here. Briefly, the five native cysteines were replaced with C18L, C43S, C167V, C178A, and C612A, and a Cys-free mutant was made. Then, eight different Cys-light mutants were produced, each containing a single cysteine (pRepS43C, pRepA333C, pRepS316C, pRepA310C, pRepS233C, pRepA97C, pRepA473C, and pRepS486C). None of these eight sites are within the known helicase motifs, they are not shared among Rep, UvrD, and PcrA, and they are well exposed on the surface of the protein, making them ideal for labeling. These Cys-light mutants were then labeled by mixing them with excess amounts of Cy3 maleimide with ~90% efficiency. The ATP hydrolysis and DNA unwinding activities of the Cys-light proteins and labeled proteins was measured and found to be at least 75% of the wild-type proteins (25).

smFRET assay

Single-molecule measurements were performed using a prism-type total internal reflection microscope (IX50, Olympus, Center Valley, PA) and an electron-multiplying charge-coupled device camera (iXon DV 887-BI EMCCD, Andor Technology, Belfast, Northern Ireland). Both the quartz slide and the glass coverslip that formed the sample chamber were coated with biotin-functionalized polyethylene glycol (PEG) to reduce nonspecific binding of DNA and proteins. All single-molecule measurements were performed in a saturated Trolox ($\approx$2 mM, Calbiochem, San Diego, CA) buffer containing an oxygen scavenging system (0.1 mg/ml glucose oxidase, 0.02 mg/ml catalase (Roche, Indianapolis, IN), 0.8% (w/w) dextrose, and 1% v/v 2-mercaptoethanol), 10 mM $MgCl_2$, 15 mM NaCl, and 0.1 mg/ml bovine serum albumin. This buffer increases the photostability and suppresses the blinking of the fluorophores. ATPγS, ADP.Vi, or ADP (500 μM each) were used as ATP hydrolysis intermediates. Fluorescence images were acquired at an integration time of 100 ms. Movies of 700–1200 frames were recorded in 8-bit format and analyzed using custom programs written in MATLAB. Finally, crystal structure data and results of our triangulation analysis were superimposed using the software Visual Molecular Dynamics. Visual Molecular Dynamics is freely available at http://www.ks.uiuc.edu/Research/vmd/.

Triangulation

Triangulation is a method in which the location of a point is determined by using the distance between this point and three other points. As in global positioning systems, three distances are the minimum required constraints to reduce the possible locations to two points, one of which is typically not relevant to the system of interest. At the molecular level, fluorescence resonance energy transfer (FRET)-based triangulation has been used to obtain structural information in physiologically relevant solution conditions (25,28–30). In our case, we measure the FRET efficiency between a Cy3-labeled residue on Rep and a Cy5-labeled nucleotide on DNA. Under these conditions, we typically get a distribution of FRET efficiency values, suggesting that a range of donor-acceptor separations is sampled for each protein-DNA pair. Multiple binding sites on DNA, the flexibility of linkers that attach the fluorophores to DNA or protein, and dynamics in the binding conformations of the Rep-DNA complex may all contribute to the distribution. Under such nonideal conditions, using more than three constraints would make the analysis more rigorous and less prone to potential error. In our case, we determine the position of a Cy5 acceptor by measuring

the FRET efficiency between this acceptor and eight independent donors distributed on various residues on Rep. We used the FRET nanopositioning (NPS) program by Muschielok et al. for this analysis (29).

RESULTS

Triangulation using the FRET NPS system

We used prism-type total internal reflection microscopy (see Fig. 2 *a* and Materials and Methods for details of the experimental assay) and smFRET-based triangulation (31). Nucleotide-free, ATPγS, ADP-vanadate (ADP.Vi), and ADP states were studied as ATP hydrolysis intermediates. ATPγS is a slowly hydrolyzable ATP analog that mimics the ATP state, and ADP.Vi mimics the ADP.Pi state (32,33). Eight Rep mutants, each labeled at a different site with a single Cy3 fluorophore (see Fig. 1 *b*), and a pdDNA labeled with a single Cy5 at the duplex-single strand junction were used (see Materials and Methods for DNA sequence and fluorophore location). Labeling sites were distributed on Rep as shown in Fig. 1 *b*: two residues within the 1A subdomain (43 and 233), one residue within the 1B subdomain (97), three residues within the 2A subdomain (310, 316, and 333) and two residues within the 2B subdomain (473 and 486). All eight single cysteine mutants are functional in vivo and in vitro (25). Initially, we studied binding of Rep with pdDNA of various tail lengths to find an optimal tail length (Supporting Material). A pdDNA with an 18-basepair (bp) duplex and a 16-nucleotide (nt) 3′-ssDNA tail (referred to as pdT16) was selected as the optimal substrate. Even though this tail length, 16 nt, is long enough in principle to accommodate two Rep monomers, the low protein concentration (1 nM) makes this unlikely. In addition, all traces were individually screened and those that showed more than one donor photobleaching step were excluded from analysis, ensuring

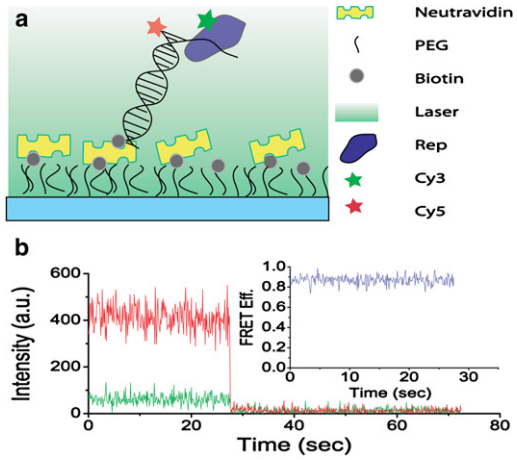

FIGURE 2 (*a*) Experimental configuration. (*b*) Representative time traces of a single Rep (donor-labeled) bound to a DNA (acceptor-labeled), with donor and acceptor intensities indicated by the green and red lines, respectively. The donor photobleaches at $t = 28$ s. (*Inset*) FRET efficiency.

binding of a single protein to DNA. Overall, eight Rep mutants and one DNA construct were studied in four different nucleotide states, resulting in 32 different FRET measurements.

Our analysis has two sets of input: donor fluorophore locations determined by Rep crystal structures; and measured FRET efficiencies between these donor fluorophores and the acceptor fluorophore. These two inputs are used to determine the location of the acceptor fluorophore, which represents the location of the DNA junction relative to Rep. We can also determine, using quantifiable metrics, whether the results are more consistent with the open or closed conformations. The check for consistency of the FRET data with the open or closed conformation is based on agreement between the junction position predicted from triangulation analysis and the location expected based on the crystal structure. This procedure was repeated for all four ATP hydrolysis intermediates.

Fig. 2 *b* shows a sample time trace of fluorescence intensities of the donor and acceptor signal for Rep labeled at residue 333 in the nucleotide-free state. Most traces have constant FRET efficiencies and do not show transitions to other FRET efficiencies. Fig. 3 shows the FRET efficiency histograms, each representing several hundred Rep-pdDNA complexes, for Rep labeled with a Cy3 at a different residue and DNA labeled with a Cy5 at the junction. Each row represents a different Rep construct (Rep43, Rep97, Rep233, Rep310, Rep316, Rep333, Rep473, and Rep486 (Fig. 3, *A–H*, respectively)), and each column represents a nucleotide state (nucleotide-free, ATPγS, ADP.Vi, and ADP (Fig. 3, *columns 1–4*, respectively). The peak positions are summarized in Table 1.

The histograms showed distributions that could be described with one or a sum of two Gaussian functions. In the nucleotide-free state, seven of eight Rep constructs showed a single peak, and in the ADP.Vi state, all eight constructs did so. In contrast, five out of eight constructs showed two peaks for both the ATPγS and ADP states, indicating at least two different conformations. Single-molecule time traces showed occasional transitions between the two states that were more frequent during the initial binding of the protein to the DNA, i.e., the protein binds in one conformation and transitions into the other conformation after a short dwell time (<1 s). Examples of these transitions are shown in Fig. S2 in the Supporting Material. It is of interest that Rep labeled on either residue in the 2B subdomain (473 and 486) shows a single peak in both the ATPγS and ADP states (see Table 1). Therefore, in the two conformations, the 2B subdomain may have the same relative position against the partial duplex junction. Because the crystal structures of UvrD and PcrA bound to a 3′-tailed pdDNA showed a 2B-dsDNA interaction, we suggest that the two conformations we observed here involve a coordinated motion of 2B and dsDNA relative to the portion of the protein composed of the 1A, 2A, and 1B subdomains.

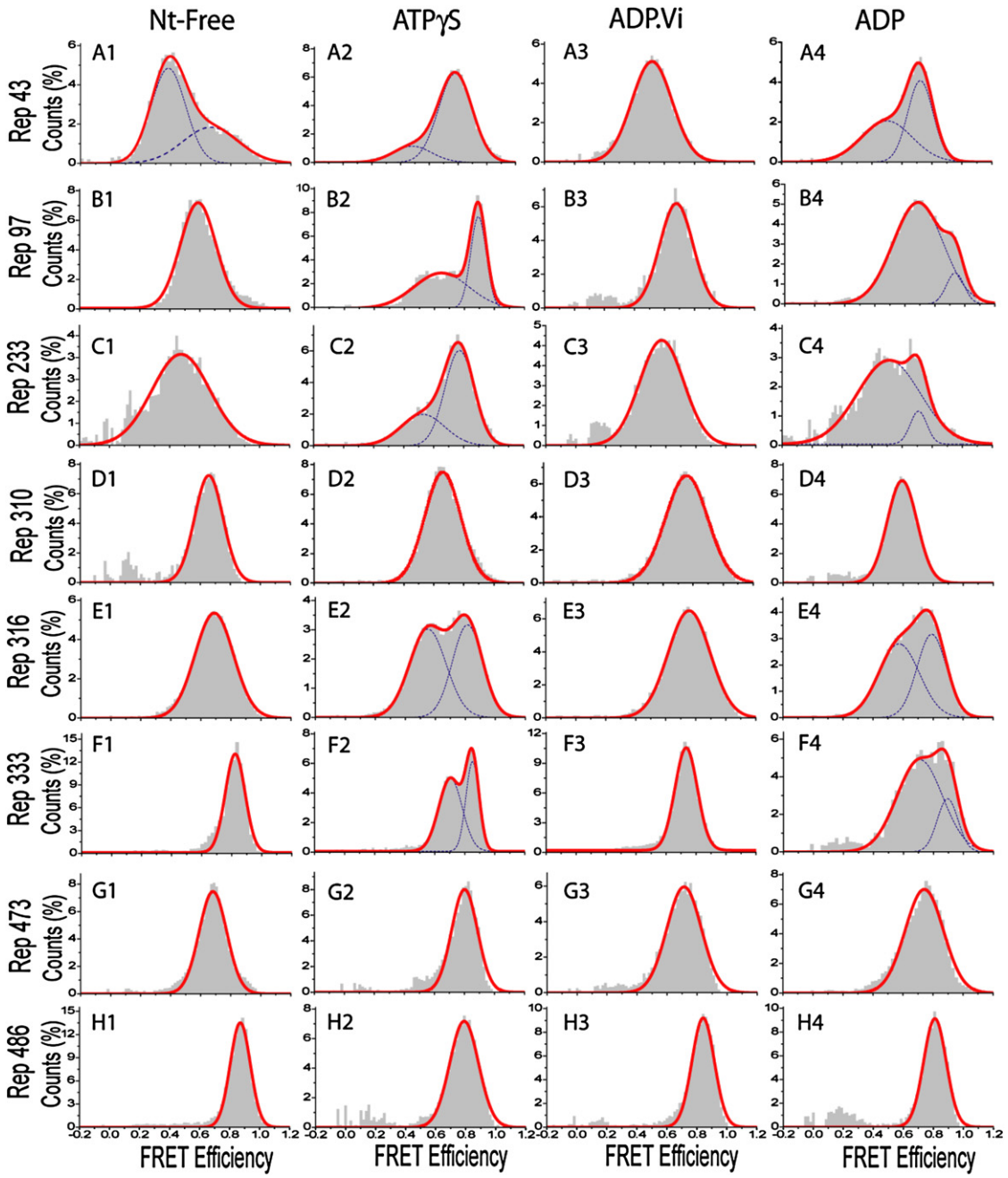

FIGURE 3 Histograms of single-molecule FRET efficiency between Cy3-labeled Rep constructs, labeled at the indicated residue number, and Cy5-labeled DNA (labeled at the junction of a pdDNA). Each row represents a Rep construct in the following order Rep43, Rep97, Rep233, Rep310, Rep316, Rep 333, 473, and Rep486 (*A–H*, respectively; see Table 1 for the subdomain each residue belongs to). Columns 1–4 represent the nucleotide-free, ATPγS, ADP.Vi, and ADP states, respectively. Single or double Gaussian fits are also shown.

The single-molecule measurements made here revealed multiple conformations not observed previously. However, the presence of multiple conformations presents a technical challenge, especially for the triangulation analysis, because in principle there are 32 (2^5) possible ways of linking two different FRET states for each of the five Rep constructs that showed two populations. At present, to our knowledge, there is no generalizable solution for this problem. In an earlier study, Choi et al. (34) chose the FRET state with the dominant population for each construct to perform triangulation for the major population. However, in our case, the two FRET states show similar populations for most constructs. Instead, we assumed that one of the two conformations in the ATPγS or ADP states is similar to that of the ADP.Vi state (primary conformation). Going on this assumption, we picked the FRET states with FRET values

TABLE 1 Summary of FRET peaks

Residue domain	Res 43 (1A)	Res 97 (1B)	Res 233 (1A)	Res 310 (2A)	Res 316 (2A)	Res 333 (2A)	Res 473 (2B)	Res 486 (2B)
Nt-free	0.38/0.67	0.59	0.48	0.66	0.69	0.82	0.68	0.87
ATPgS	0.48/0.78	0.65/0.89	0.53/0.77	0.66	0.55/0.81	0.70/0.85	0.80	0.79
ADPVi	0.52	0.68	0.57	0.76	0.76	0.73	0.71	0.84
ADP	0.50/0.72	0.69/0.94	0.51/0.71	0.59	0.57/0.79	0.71/0.89	0.74	0.81

FRET efficiency peaks for all 32 measurements are shown. In the cases where two Gaussians were required to fit the data, the corresponding peaks are separated by a slash, e.g., 0.38/0.67 means that the data were fit by two Gaussians centered at FRET efficiency values of 0.38 and 0.67. Res, residue.

closer to those of the ADP.Vi values and grouped them into Set 1. The remaining FRET states were grouped into Set 2. The residues that have a single peak are grouped in both sets. For example, for the residue 43 ATPγS state, the two peaks are 0.48 and 0.78. The ADP.Vi peak for residue 43 is 0.52. Since 0.48 is closer to 0.52, it is grouped into Set 1 and 0.78 is grouped into Set 2. Hence, Set 1 for the ATPγS state is (in increasing order of residue numbers) {0.48, 0.65, 0.53, 0.66, 0.81, 0.70, 0.80, 0.79} and Set 2 is {0.78, 0.89, 0.77, 0.66, 0.55, 0.85, 0.80, 0.79}. In a similar way, Set 1 of ADP is {0.50, 0.69, 0.51, 0.59, 0.79, 0.71, 0.74, 0.81} and Set 2 is {0.72, 0.94, 0.71, 0.59, 0.57, 0.89, 0.74, 0.81}.

Triangulation analysis was then applied to each set to determine the junction position relative to the protein using the method developed by Muschielok et al. (29). The method is called FRET NPS, and it employs a Bayesian algorithm to calculate the most likely position, e.g., the position(s) at which the probability distribution has the maximum value, and the probability distribution of possible positions. In our case, we used eight FRET values and FRET NPS to determine the position of the acceptor fluorophore, hence the DNA junction, and the uncertainty associated with this position. The uncertainty arises from several factors including the uncertainty in the measured FRET values, the available volume for the fluorophore on the protein surface, the length of the linker connecting the fluorophore to the protein or to the DNA, and the distribution of the Förster radius. To estimate the uncertainty, we modeled each donor position based on the Rep crystal structure to determine the available volume for each fluorophore. In addition, we used an uncertainty of ± 0.05 for all experimental FRET efficiency values, and we modeled the distribution of the Förster radius for each donor-acceptor pair based on anisotropy measurements of the corresponding labeling site on the protein. Finally, we used a linker length of 5 Å for both the Cy3-Rep linker and the Cy5-DNA linker.

The results for Set 1 of the ADP state are shown in Fig. 4, with the Rep structure in the closed (*white mesh*) and open (*cyan mesh*) conformations (Fig. 4, *a* and *b*, respectively), and with the 2B residues excluded from the analysis (*orange mesh*) (Fig. 4 *c*). The mesh structure represents an envelope of possible locations determined using an isovalue of 1.0, which corresponds to the smallest possible envelope that encloses the sought position with 68% certainty. Imposing a smaller isovalue results in a larger envelope, as higher certainty is required. Due to the difficulty of conveying the 3D distribution as a 2D projection in a figure, we refer the reader to 360° videos in the Supporting Material.

The common characteristic of all the nucleotide states is that when the 2B residues are not included in the analysis, the probability density spans a broad arch, as in Fig. 4 *c*. Including the 2B residues in the closed or open conformations localizes this arch into a single small pocket (as in Fig. 4 *a*) or into two small pockets (as in Fig. 4 *b*). If we then increase the isovalue, both envelopes shrink, but one disappears earlier than the other. What remains as we increase the isovalue is considered the most likely pocket. In this way, we determined the most likely position for all nucleotide states and conformations (Fig. 5, *a* and *b*, and Table 2). As discussed in detail at the end of this section, the mesh size can be taken as an indicator of resolution, and the most likely positions are used to infer whether our data are more consistent with the open or closed conformation, as we discuss next.

Comparison to open and closed conformations

We performed two related analyses to decide whether the open or closed conformation is more consistent with our data. The first analysis is based on the distance between the most likely junction position (Table 2) and the 5′ end of the ssDNA in the crystal structure of Rep. These distances are given in the third column of Table 2. Because our DNA is a 3′-tailed partial duplex, we expect that the partial duplex junction will be close to the 5′ end of the ssDNA seen in the crystal structure of Rep. The junction positions predicted by the closed conformation are concentrated in a region 19 Å

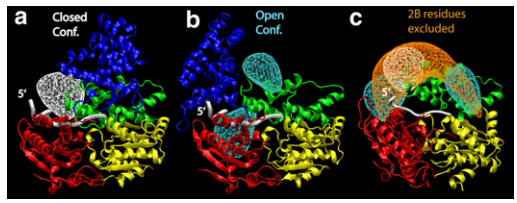

FIGURE 4 Probability distributions of optimal positions of the Cy5-labeled junction predicted by triangulation analysis, using FRET NPS, for the ADP state (Set 1), with Rep subdomains 1A, 2A, 1B, and 2B in yellow, red, green, and blue, respectively. The predictions for (*a*) the closed conformation (*white mesh*) and (*b*) the open conformation (*cyan mesh*) are shown. (*c*) 2B residues are excluded from the analysis (*orange mesh*), and the results for the open (*cyan*) and closed (*white*) conformations are also shown for comparison.

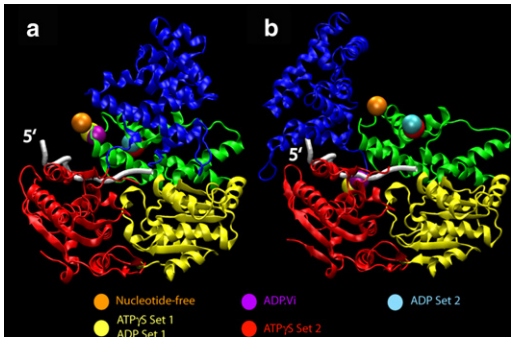

FIGURE 5 Most likely positions of the Cy5-labeled junction for (*a*) the closed and (*b*) the open conformations for all nucleotide states are shown as spheres colored yellow for Set 1 of ATPγS and Set 1 of ADP (represented by a single sphere, as they are exactly the same), orange for the nucleotide-free state, purple for ADP.Vi, red for ATPγS Set 2, and cyan for ADP Set 2. Rep subdomains 1A, 2A, 1B, and 2B are in yellow, red, green, and blue, respectively.

away from the 5′ end of the ssDNA. On the other hand, the junction positions predicted by the open conformation are populated in two regions both of which are ~32 Å away from the 5′ end of ssDNA. The 19-Å deviation in the closed conformation is within the uncertainty dictated by the dsDNA diameter and the linker.

In the second analysis, the junction position determined for the closed conformation of Rep is compared with that obtained in the crystal structures of UvrD-pdDNA complexes. To facilitate this comparison we mapped the UvrD-pdDNA complex onto the Rep-ssDNA complex based on the α-carbons in the 1A and 2A subdomains of the two proteins. Fig. 6 shows this mapping, along with the fluorophore position predicted from our triangulation

TABLE 2 Comparison of open- and closed-conformation results

State	Most likely position	Distance to 5′ end (Å)	Distance to junction (Å)
Closed conformation			
Nt-free	(24,10,90)	17	14
ATPγS-1	(20,12,90)	20	16
ATPγS-2	(16,24,94)	27	26
ADPVi	(20,14,90)	19	16
ADP-1	(20,12,90)	20	16
ADP-2	(18,24,94)	25	25
Open conformation			
Nt-free	(58,36,88)	32	44
ATPγS-1	(2,12,80)	34	25
ATPγS-2	(44,42,92)	31	42
ADPVi	(4,14,82)	32	24
ADP-1	(2,12,80)	34	25
ADP-2	(46,42,92)	32	43

The most likely positions, and distances from these positions to the 5′ end of ssDNA, for the open and closed conformations. The last column gives the distance from the most likely positions to the junction position estimated from UvrD-Rep mapping (Fig. 6).

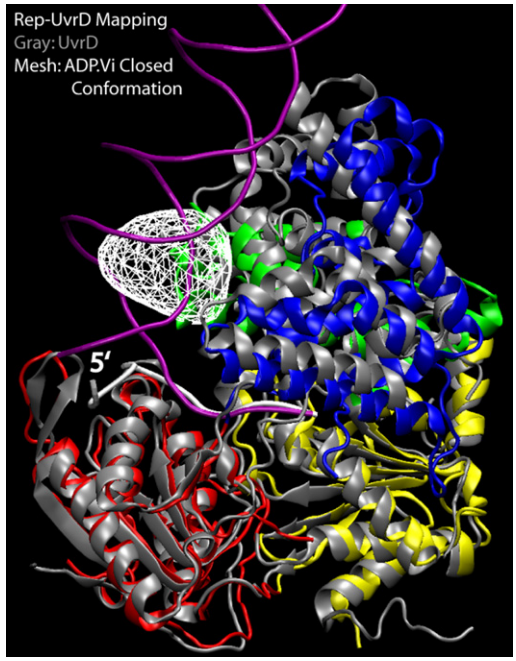

FIGURE 6 UvrD-pdDNA complex mapped onto Rep. The prediction of the junction position for the closed conformation is shown in white mesh for the ADP.Vi state, and Rep subdomains are color-coded as in other figures.

analysis. UvrD is shown in gray, the pdDNA in magenta, the predicted position for the ADP.Vi state in white mesh, and the Rep domains in the same colors used in other figures. As can be inferred from Table 2,the most likely positions for the other nucleotide states of the closed conformation would also occur in similar positions. As shown in Fig. 6, there are remarkable structural similarities between the two proteins. In fact, even such a simple mapping results in an almost identical path for ssDNA within the two helicases (data not shown). The ssDNA-dsDNA junction position, assumed to be the center point of the 20-Å-wide dsDNA, is 16 Å from the predicted position for the closed conformation. Given that the fluorophore is attached to the junction via a 5-Å-long linker and that we are comparing two similar but different helicases, the 16-Å distance between the two positions is an acceptable result. A similar analysis using the open conformation data gave significantly larger deviations, ranging between 25 and 44 Å for different nucleotide states (Table 2, *last column*). This analysis further supports the better consistency of the closed conformation with our data.

Multiple conformations for ATPγS or ADP

An interesting and unexpected finding of this study is that we observe multiple conformations of the Rep-DNA complex in the ATPγS and ADP-bound states. Here, we consider these multiple conformations in more detail, focusing on the closed conformation, because it is more

consistent with our data. The predicted junction positions for Set 1 of the ATPγS data and Set 1 of the ADP data are identical to each other and are in close proximity to (within 6 Å of) the positions predicted by the nucleotide-free and ADP.Vi states (see Table 2). This is expected given the choices made in selecting Set 1. The positions predicted by Set 2 of the ATPγS data and Set 2 of the ADP data are also almost identical to each other (2-Å deviation), but are significantly different, by ~15 Å, from the positions prevalent in the other nucleotide states. Furthermore, the junction positions predicted by Set 1 and Set 2 differ by ~15 Å, which is much larger than what one would expect from rearrangement of the two RecA-like domains of Rep during ATP binding and hydrolysis. Therefore, these two cases should be considered different conformations of the Rep-pdDNA complex, and they will be referred to as the primary (result of Set 1 peaks) and secondary (result of Set 2 peaks) conformations. It is interesting to note that the residues in the 1A, 1B, and 2A subdomains all show double FRET peaks when bound to ATPγS and ADP, whereas the residues within the 2B subdomain show only single FRET peaks in these nucleotide states (see Table 1). According to our interpretation, this indicates that the 2B subdomain moves in synchrony with the duplex DNA and hence has the same relative distance to the junction in both conformations, resulting in a single FRET peak. On the other hand, the other subdomains move relative to the duplex DNA in the primary and secondary conformations.

The different junction positions predicted for the primary and secondary conformations are also reflected in the distances from these positions to the 5′ end of ssDNA or to the junction position predicted from Rep UvrD mapping (Table 2, *last two columns*). In addition to these quantitative differences, the positions predicted by the secondary conformation (Set 2) in the ATPγS and ADP states are buried within the 1B subdomain of Rep, which is not an acceptable position for the junction. Therefore, the secondary conformation is likely to be significantly different from what is observed in the crystallographic structures. One possibility is that the 2B subdomain itself may have an orientation distinct from both the open and closed conformations. A clash between the predicted junction location and the 1B subdomain also exists for the primary conformation but to a much smaller extent. In the primary conformation case, the most likely position is outside the 1B subdomain and does not clash with it, even though the mesh volume partially overlaps with the 1B subdomain(Fig. 4 *a*). Therefore, the primary conformation we deduced here is consistent with the closed conformation of Rep observed in the crystal structure.

DISCUSSION

We have interpreted the surprising finding of two FRET populations for the 1A, 1B, and 2A subdomain residues in the ATPγS and ADP states as indicating that multiple conformations are present in these nucleotide states. The single FRET populations in the 2B residues (473 and 486) have motivated the interpretation of a coordinated movement of the 2B subdomain with the duplex DNA. As the acceptor fluorophore is located at the ss/dsDNA junction, alternative scenarios including junction dynamics or dsDNA melting at the junction should be discussed as alternative explanations for our data. The first scenario to consider is whether junction dynamics, e.g., junction stabilizing in two different locations or transitioning between two different locations while Rep remains essentially static, could be the reason for multiple FRET peaks. In this scenario, as Rep is static while the junction is moving, we would expect multiple FRET populations for all residues regardless of where on Rep they are located. However, our data show multiple populations for 1A, 1B, and 2A residues, whereas the 2B residues demonstrate a single population, making this scenario unlikely.

Another scenario to consider is whether different levels of Rep-induced duplex junction melting in different nucleotide states could result in multiple FRET peaks or influence the FRET results in significant ways. Numerous single-molecule measurements have been performed on Rep-pdDNA complexes and junction melting due to Rep monomer binding has not been observed to take place at detectable levels (17,25). In addition, crystal structure studies on UvrD and PcrA in complex with pdDNA and different ATP hydrolysis intermediates do not show any junction melting upon helicase binding. Even if we consider melting of a basepair at the junction, the junction would be displaced by ~3 Å from the Rep helicase. This would not be adequate to explain the 13-Å separation we observe between the primary and secondary conformations. In fact, 13 Å separation would require four to five basepairs to unwind upon Rep binding, which has not been observed previously. Finally, junction melting would affect all the Rep mutants similarly, regardless of where the fluorophore is, hence the difference in behavior between the 2B and non-2B residues cannot be explained by this scenario either.

Another possibility to consider is whether partial occupancy of ATPγS, i.e., binding to some Rep monomers but not others, could be the reason for two conformations in the ATPγS states. As we demonstrate in Fig. S3, 10 μM ATPγS is enough to saturate Rep binding, and at the experimental concentration we use, 500 μM ATPγS, all Rep molecules should be bound by ATPγS. These results are consistent with earlier bulk measurements (35,36).A related scenario that could be considered is whether slow ATPγS hydrolysis gives rise to two different conformations. Single-molecule traces do show occasional transitions between the two FRET states for some Rep constructs (Rep 43, 97, 233, 316, and 333), as demonstrated in Fig. S2, but not all of them (not observed for Rep 310, 473, and 486). If ATPγS hydrolysis were the reason for

the observed dynamics, we would have expected to observe it for all constructs. Hence, we do not think this scenario is consistent with our data.

An important question that should be considered is what the potential biological significance is for having two conformational states in the ATPγS and ADP states whereas a single conformation is observed in the ADP.Vi state. Because the ATPase reaction would proceed from the ATPγS state to the ADP.Vi state and then to the ADP state, we can speculate that the ATPase reaction may proceed in two pathways upon ATP binding. The two pathways would then merge upon ATP hydrolysis and then diverge again when Pi is released. These multiple pathways may provide a mechanism of regulation of helicase activity, depending on the functional context. If multiple pathways and conformations already exist in the enzyme-DNA complex, one can imagine that changes in the environment or functional context can enable the selection of one of the existing conformations without having to induce a new conformation.

The resolution of our method can be estimated from the size of the mesh structures, i.e., the size of one of the pockets of probability distribution in Fig. 4 *a*. The resolution is characterized quantitatively by the standard deviation of the most likely position of the probability distribution. For the closed conformation, a single pocket of probability distribution is obtained in five of six cases, whereas this number is two of six for the open conformation. The fact that it resulted in a broader probability distribution compared to the closed conformation is another reason why the open conformation is less likely. In all single-pocket cases of the closed conformation, the mesh structures have a standard deviation of ~10 Å, which corresponds to a standard deviation of ~6 Å in the *x*-, *y*-, and *z*-directions.

Finally, we can examine the consistency of the triangulation analysis by including different numbers of residues in the analysis using the ADP state as an example. The standard deviation in the most likely position of the junction gradually increases from 8 Å to 12 Å when the number of residues is decreased from eight to three, ~1 Å per eliminated residue. However, using five residues or less resulted in a second pocket appearing in the probability distribution for all studied cases. Not including both 2B residues in analysis was an exception, as it resulted in an abrupt decrease in resolution, which we believe is due to nonuniform distribution of the labeled residues. On the other hand, the most likely positions did not change significantly regardless of the number of constraints used, and they were all within 8 Å of each other, demonstrating the robustness of the analysis and consistency of the data.

CONCLUSIONS

This study has several important conclusions for the conformational state of Rep helicase when in complex with pdDNA and an ATP hydrolysis intermediate (nucleotide-free, ATPγS, ADP.Pi, and ADP studied). First of all, for all ATP hydrolysis intermediate states, our data are more consistent with Rep being in a closed conformation, with respect to its 2B subdomain, than in the open conformation. This conclusion is also consistent with the crystal structure studies on related helicases such as UvrD and PcrA. However, we show that in the ATPγS and ADP bound states the Rep-pdDNA complex shows evidence of at least two conformations, whereas the crystal structures of UvrD showed only one conformation. Hence, studies of static crystal structures do not capture the fully dynamic aspects of this complex under these conditions. During this reconfiguration between the two conformations, the 2B subdomain rotates with the duplex DNA. This may result in a tension change between the single-stranded portion and the enzyme's motor domains (2A and 1A), although at present we do not know the functional roles of these movements. One speculation as to the biological significance of having multiple conformations is that they allow selection of one pathway over another, which could in turn regulate helicase activity, depending on the environmental conditions or functional context, without having to induce new conformational states. Finally, we demonstrate that FRET-based triangulation analysis is capable of providing 10-Å resolution in the absolute position, which should be enough to address many other biological questions. In particular, we believe that a triangulation analysis would be particularly powerful in structural problems involving multiple biological entities (34), e.g., dimerization conformation of two proteins or assembly conformation of a multiprotein complex on a DNA substrate, since such problems could be very difficult to address using more conventional methods, such as x-ray crystallography.

SUPPORTING MATERIAL

Three figures and 13 movies are available at http://www.biophysj.org/biophysj/supplemental/S0006-3495(11)00840-X.

We thank Professors Jens Michaelis and Adam Muschielok for their insightful comments.

Funds were provided by the National Institutes of Health (GM-065367 to T.H. and GM-045948 to T.M.L.).

REFERENCES

1. Lohman, T. M., and K. P. Bjornson. 1996. Mechanisms of helicase-catalyzed DNA unwinding. *Annu. Rev. Biochem.* 65:169–214.
2. Patel, S. S., and K. M. Picha. 2000. Structure and function of hexameric helicases. *Annu. Rev. Biochem.* 69:651–697.
3. Singleton, M. R., M. S. Dillingham, and D. B. Wigley. 2007. Structure and mechanism of helicases and nucleic acid translocases. *Annu. Rev. Biochem.* 76:23–50.
4. Lohman, T. M., E. J. Tomko, and C. G. Wu. 2008. Non-hexameric DNA helicases and translocases: mechanisms and regulation. *Nat. Rev. Mol. Cell Biol.* 9:391–401.

5. Cordin, O., J. Banroques, …, P. Linder. 2006. The DEAD-box protein family of RNA helicases. *Gene.* 367:17–37.
6. Delagoutte, E., and P. H. von Hippel. 2003. Helicase mechanisms and the coupling of helicases within macromolecular machines. Part II: Integration of helicases into cellular processes. *Q. Rev. Biophys.* 36: 1–69.
7. Matson, S. W., D. W. Bean, and J. W. George. 1994. DNA helicases: enzymes with essential roles in all aspects of DNA metabolism. *Bioessays.* 16:13–22.
8. Saha, A., J. Wittmeyer, and B. R. Cairns. 2006. Chromatin remodelling: the industrial revolution of DNA around histones. *Nat. Rev. Mol. Cell Biol.* 7:437–447.
9. Veaute, X., S. Delmas, …, M. A. Petit. 2005. UvrD helicase, unlike Rep helicase, dismantles RecA nucleoprotein filaments in *Escherichia coli*. *EMBO J.* 24:180–189.
10. Ellis, N. A. 1997. DNA helicases in inherited human disorders. *Curr. Opin. Genet. Dev.* 7:354–363.
11. Korolev, S., J. Hsieh, …, G. Waksman. 1997. Major domain swiveling revealed by the crystal structures of complexes of *E. coli* Rep helicase bound to single-stranded DNA and ADP. *Cell.* 90:635–647.
12. Subramanya, H. S., L. E. Bird, …, D. B. Wigley. 1996. Crystal structure of a DExx box DNA helicase. *Nature.* 384:379–383.
13. Velankar, S. S., P. Soultanas, …, D. B. Wigley. 1999. Crystal structures of complexes of PcrA DNA helicase with a DNA substrate indicate an inchworm mechanism. *Cell.* 97:75–84.
14. Brendza, K. M., W. Cheng, …, T. M. Lohman. 2005. Autoinhibition of *Escherichia coli* Rep monomer helicase activity by its 2B subdomain. *Proc. Natl. Acad. Sci. USA.* 102:10076–10081.
15. Dillingham, M. S., D. B. Wigley, and M. R. Webb. 2002. Direct measurement of single-stranded DNA translocation by PcrA helicase using the fluorescent base analogue 2-aminopurine. *Biochemistry.* 41:643–651.
16. Fischer, C. J., N. K. Maluf, and T. M. Lohman. 2004. Mechanism of ATP-dependent translocation of *E. coli* UvrD monomers along single-stranded DNA. *J. Mol. Biol.* 344:1287–1309.
17. Myong, S., I. Rasnik, …, T. Ha. 2005. Repetitive shuttling of a motor protein on DNA. *Nature.* 437:1321–1325.
18. Niedziela-Majka, A., M. A. Chesnik, …, T. M. Lohman. 2007. *Bacillus stearothermophilus* PcrA monomer is a single-stranded DNA translocase but not a processive helicase in vitro. *J. Biol. Chem.* 282: 27076–27085.
19. Tomko, E. J., C. J. Fischer, …, T. M. Lohman. 2007. A nonuniform stepping mechanism for *E. coli* UvrD monomer translocation along single-stranded DNA. *Mol. Cell.* 26:335–347.
20. Cheng, W., J. Hsieh, …, T. M. Lohman. 2001. *E. coli* Rep oligomers are required to initiate DNA unwinding in vitro. *J. Mol. Biol.* 310:327–350.
21. Maluf, N. K., C. J. Fischer, and T. M. Lohman. 2003. A Dimer of *Escherichia coli* UvrD is the active form of the helicase in vitro. *J. Mol. Biol.* 325:913–935.
22. Jia, H., S. Korolev, …, T. M. Lohman. 2011. Rotations of the 2B Subdomain of E. coli UvrD Helicase/Translocase Coupled to Nucleotide and DNA Binding. *J. Mol. Biol.* 10.1016/j.jmb.2011.06.019.
23. Lee, J. Y., and W. Yang. 2006. UvrD helicase unwinds DNA one base pair at a time by a two-part power stroke. *Cell.* 127:1349–1360.
24. Cheng, W., K. M. Brendza, …, T. M. Lohman. 2002. The 2B domain of the *Escherichia coli* Rep protein is not required for DNA helicase activity. *Proc. Natl. Acad. Sci. USA.* 99:16006–16011.
25. Rasnik, I., S. Myong, …, T. Ha. 2004. DNA-binding orientation and domain conformation of the *E. coli* rep helicase monomer bound to a partial duplex junction: single-molecule studies of fluorescently labeled enzymes. *J. Mol. Biol.* 336:395–408.
26. Park, J., S. Myong, …, T. Ha. 2010. PcrA helicase dismantles RecA filaments by reeling in DNA in uniform steps. *Cell.* 142:544–555.
27. Tomko, E. J., H. Jia, …, T. M. Lohman. 2010. 5′-Single-stranded/duplex DNA junctions are loading sites for *E. coli* UvrD translocase. *EMBO J.* 29:3826–3839.
28. Andrecka, J., R. Lewis, …, J. Michaelis. 2008. Single-molecule tracking of mRNA exiting from RNA polymerase II. *Proc. Natl. Acad. Sci. USA.* 105:135–140.
29. Muschielok, A., J. Andrecka, …, J. Michaelis. 2008. A nano-positioning system for macromolecular structural analysis. *Nat. Methods.* 5:965–971.
30. Sun, X., D. F. Mierke, …, M. Radman-Livaja. 2006. Architecture of the 99 bp DNA-six-protein regulatory complex of the lambda att site. *Mol. Cell.* 24:569–580.
31. Ha, T., T. Enderle, …, S. Weiss. 1996. Probing the interaction between two single molecules: fluorescence resonance energy transfer between a single donor and a single acceptor. *Proc. Natl. Acad. Sci. USA.* 93:6264–6268.
32. Lindquist, R. N., J. L. Lynn, Jr., and G. E. Lienhard. 1973. Possible transition-state analogs for ribonuclease. The complexes of uridine with oxovanadium(IV) ion and vanadium(V) ion. *J. Am. Chem. Soc.* 95:8762–8768.
33. Westheimer, F. H. 1987. Why nature chose phosphates. *Science.* 235: 1173–1178.
34. Choi, U. B., P. Strop, …, K. R. Weninger. 2010. Single-molecule FRET-derived model of the synaptotagmin 1-SNARE fusion complex. *Nat. Struct. Mol. Biol.* 17:318–324.
35. Moore, K. J., and T. M. Lohman. 1994. Kinetic mechanism of adenine nucleotide binding to and hydrolysis by the *Escherichia coli* Rep monomer. 2. Application of a kinetic competition approach. *Biochemistry.* 33:14565–14578.
36. Moore, K. J., and T. M. Lohman. 1994. Kinetic mechanism of adenine nucleotide binding to and hydrolysis by the *Escherichia coli* Rep monomer. 1. Use of fluorescent nucleotide analogues. *Biochemistry.* 33:14550–14564.